Čerenkov-type second-harmonic spectroscopy in random nonlinear photonic structures

Mousa Ayoub,[1,*] **Philip Roedig,**[1] **Kaloian Koynov,**[2] **Jörg Imbrock,**[1] **and Cornelia Denz**[1]

[1]*Institute of Applied Physics and Center for Nonlinear Science (CeNoS), University of Münster, Corrensstr. 2, 48149 Münster, Germany*

[2]*Max Planck Institute for Polymer Research, Ackermannweg 10, 55128, Mainz, Germany*

[*]*ayoubm@uni-muenster.de*

Abstract: We report on experimental and theoretical studies of Čerenkov-type second-harmonic generation in random nonlinear photonic structures with different two-dimensional distributions of the ferroelectric domains. We utilize Čerenkov-type second-harmonic generation spectroscopy to estimate the average ferroelectric domain size by analyzing the spatial Fourier spectrum of the domain patterns. This is measured by scanning the Čerenkov second-harmonic signal for different angles of incidence and light polarizations of the fundamental wave. By comparing the experimental results with numerically simulated Fourier spectra, the corresponding domain patterns are retrieved, which are in a good correspondence with images obtained by Čerenkov-type second-harmonic generation microscopy.

OCIS codes: (190.4410) Nonlinear optics, parametric processes; (190.4420) Nonlinear optics, transverse effects in; (190.4400) Nonlinear optics, materials.

References and links

1. S. Kawai, T. Ogawa, H. S. Lee, R. C. DeMattei, and R. S. Feigelson, "Second-harmonic generation from needle-like ferroelectric domains in $Sr_{0.6}Ba_{0.4}Nd_2O_6$ single crystals," Appl. Phys. Lett. **73**, 768–770 (1998).
2. E. Y. Morozov, A. A. Kaminski, A. S. Chirkin, and D. B. Yusupov, "Second optical harmonic generation in nonlinear crystals with a disordered domain structure," JETP Lett. **73**, 647–650 (2001).
3. M. Baudrier-Raybaut, R. Haidar, P. Kupecek, P. Lemasson, and E. Rosencher, "Random quasi-phase-matching in bulk polycrystalline isotropic nonlinear materials," Nature **432**, 374–376 (2004).
4. K. A. Kuznetsov, G. K. Kitaeva, A. V. Shevlyuga, L. I. Ivleva, and T. R. Volk, "Second harmonic generation in a strontium barium niobate crystal with a random domain structure," JETP Letters **87**, 98–102 (2008).
5. P. Molina, S. Álvarez García, M. O. Ramírez, J. García-Solé, L. E. Bausá, H. Zhang, W. Gao, J. Wang, and M. Jiang, "Nonlinear prism based on the natural ferroelectric domain structure in calcium barium niobate," Appl. Phys. Lett. **94**, 071111(1)–071111(3) (2009).
6. K. Kalinowski, V. Roppo, T. Lukasiewicz, M. Swirkowicz, Y. Sheng, and W. Krolikowski, "Parametric wave interaction in one-dimensional nonlinear photonic crystal with randomized distribution of second-order nonlinearity," Appl. Phys. B **109**, 557–566 (2012).
7. R. Fischer, S. M. Saltiel, D. N. Neshev, W. Krolikowski, and Y. S. Kivshar, "Broadband femtosecond frequency doubling in random media," Appl. Phys. Lett. **89**, 191105(1)–191105(3) (2006).
8. W. Wang, V. Roppo, K. Kalinowski, Y. Kong, D. N. Neshev, C. Cojocaru, J. Trull, R. Vilaseca, K. Staliunas, W. Krolikowski, S. M. Saltiel, and Y. Kivshar, "Third-harmonic generation via broadband cascading in disordered quadratic nonlinear media," Optics Express **17**, 20117–20123 (2009).
9. M. Ayoub, J. Imbrock, and C. Denz, "Second harmonic generation in multi-domain χ^2 media: from disorder to order," Opt. Express **19**, 11340–11354 (2011).

#181210 - $15.00 USD Received 5 Dec 2012; revised 15 Feb 2013; accepted 3 Mar 2013; published 28 Mar 2013

10. A. R. Tunyagi, M. Ulex, and K. Betzler, "Noncollinear optical frequency doubling in strontium barium niobate," Phys. Rev. Lett. **90**, 243901(1)–243901(4) (2003).
11. X. Vidal and J. Martorell, "Generation of light in media with a random distribution of nonlinear domains," Phys. Rev. Lett. **97**, 013902(1)–013902(4) (2006).
12. P. Molina, M. de la O Ramírez, and L. E. Bausá, "Strontium barium niobate as a multifunctional two-dimensional nonlinear photonic glass," Adv. Funct. Mater. **18**, 709–715 (2008).
13. V. Vaičaitis, "Cherenkov-type phase matching in bulk KDP crystal," Opt. Commun. **209**, 485–490 (2002).
14. Y. Zhang, X. P. Hu, G. Zhao, S. N. Zhu, and M. Xiao, "Cerenkov second-harmonic arc from a hexagonally poled $LiTaO_3$ planar waveguide," J. Phys. D **42**, 215103–215107 (2009).
15. S. M. Saltiel, Y. Sheng, N. Voloch-Bloch, D. N. Neshev, W. Krolikowski, A. Arie, K. Koynov, and Y. S. Kivshar, "Cerenkov-type second-harmonic generation in two-dimensional nonlinear photonic structures," IEEE J. Quantum. Electron. **45**, 1465–1472 (2009).
16. X. Deng, H. Ren, H. Lao, and X. Chen, "Research on Cherenkov second-harmonic generation in periodically poled lithium niobate by femtosecond pulses," J. Opt. Soc. Am. B **27**, 1475–1480 (2010).
17. J. V. Jelley, *Čerenkov Radiation and its Application* (Pergamon Press, 1958).
18. H. Ren, X. Deng, and X. Chen, "Coherently superposed efficient second harmonic generation by domain wall series in ferroelectrics," arxiv:1010.1593v1 (2010).
19. X. Deng and X. Chen, "Domain wall characterization in ferroelectrics by using localized nonlinearities," Opt. Express **18**, 15599–15602 (2010).
20. Y. Sheng, A. Best, H.-J. Butt, W. Krolikowski, A. Arie, and K. Koynov, "Three-dimensional ferroelectric domain visualization by cerenkov-type second harmonic generation," Opt. Express **18**, 16539–16545 (2010).
21. J. Bravo-Abad, X. Vidal, J. L. D. Jurez, and J. Martorell, "Optical second-harmonic scattering from a non-diffusive random distribution of nonlinear domains," Opt. Express **18**, 14202–14211 (2010).
22. M. Ayoub, P. Roedig, J. Imbrock, and C. Denz, "Domain-shape-based modulation of Čerenkov second-harmonic generation in multidomain strontium barium niobate," Opt. Lett. **36**, 4371–4373 (2011).
23. M. Ayoub, P. Roedig, J. Imbrock, and C. Denz, "Cascaded Čerenkov third-harmonic generation in random quadratic media," Appl. Phys. Lett. **99**, 241109(1)–241109(3) (2011).
24. F. Sibbers, J. Imbrock, and C. Denz, "Sum-frequency generation in disordered quadratic nonlinear media," Proc. of SPIE **7728**, 77280Y–1 (2010).
25. H. X. Li, S. Y. Mu, P. Xu, M. L. Zhong, C. D. Chen, X. P. Hu, W. N. Cui, and S. N. Zhu, "Multicolor cerenkov conical beams generation by cascaded-$\chi^{(2)}$ processes in radially poled nonlinear photonic crystals," Appl. Phys. Lett. **100**, 101101(1)–101101(4) (2012).
26. K. Kalinowski, P. Roedig, Y. Sheng, M. Ayoub, J. Imbrock, C. Denz, and W. Krolikowski, "Enhanced Čerenkov second-harmonic emission in nonlinear photonic structures," Opt. Lett. **37**, 1832–1834 (2012).
27. A. Fragemann, V. Pasiskevicius, and F. Laurell, "Second-order nonlinearities in the domain walls of periodically poled $KTiOPO_4$," Appl. Phys. Lett. **85**, 375–377 (2004).
28. S. M. Russell, P. E. Powers, M. J. Missey, and K. L. Schepler, "Broadband mid-infrared generation with two-dimensional quasi-phase-matched structures," J. Quantum Electronics **37**, 877–887 (2001).
29. A. Arie and N. Voloch, "Periodic, quasi-periodic, and random quadratic nonlinear photonic crystals," Laser and Photon. Rev. **4**, 355373 (2010).
30. M. M. Fejer, G. A. Magel, D. H. Jundt, and R. L. Byer, "Quasi-phase-matched second harmonic generation: Tuning and tolerances," IEEE J. Quantum. Electron. **28**, 2631–2654 (1992).
31. Y. Le Grand, D. Rouede, C. Odin, R. Aubry, and S. Mattauch, "Second-harmonic scattering by domains in RbH_2PO_4 ferroelectrics," Opt. Commun. **200**, 249–260 (2001).
32. U. Voelker, U. Heine, C. Gödecker, and K. Betzler, "Domain size effects in a uniaxial ferroelectric relaxor system: The case of $Sr_xBa_{1-x}Nb_2O_6$," J. Appl. Phys. **102**, 114112(1)–114112(5) (2007).
33. L. Tian, D. A. Scrymgeour, and V. Gopalan, "Real-time study of domain dynamics in ferroelectric $Sr_{0.61}Ba_{0.39}Nb_2O_6$," J. Appl. Phys. **97**, 114111(1)–114111(7) (2005).
34. M. Horowitz, A. Bekker, and B. Fischer, "Broadband second-harmonic generation in $Sr_xBa_{1x}Nb_2O_6$ by spread spectrum phase matching with controllable domain gratings," Appl. Phys. Lett. **62**, 2619–2621 (1993).

1. Introduction

In recent years, much attention has been devoted to investigate second-harmonic generation via quasi-phase matching in crystals with a random distribution of their ferroelectric domains, i.e. with a random distribution of the $\chi^{(2)}$ nonlinearity [1–6]. This new class of random nonlinear photonic crystals offers a versatile way to realize frequency conversion processes over a wide spectral range [7–9]. Among the most interesting phase-matching schemes to achieve second-harmonic emission is the so-called Čerenkov-type phase matching which has been demonstrated in different bulk nonlinear media [10–13], waveguides [14] as well as in crystals with a

#181210 - $15.00 USD Received 5 Dec 2012; revised 15 Feb 2013; accepted 3 Mar 2013; published 28 Mar 2013

periodic, quasi-periodic, and random modulation of the $\chi^{(2)}$ nonlinearity [4, 13, 15, 16]. It is a result of light-matter interaction satisfying only the longitudinal phase-matching condition [7]. It is named so because of the close analogy with the Čerenkov effect [17]. In this well-known effect a charged particle moving in a medium induces polarization. The speed of this polarization (medium excitation) is the same as the particle velocity v_p. If this velocity is higher than the phase velocity of light v_s, the conical emission due to constructive interference at a certain angle γ given by $\cos\gamma = v_s/v_p$ can be detected. The physical origin of the existence of this phenomenon in random nonlinear photonic crystals is still ambiguous, being attributed either to reciprocal grating vectors of the $\chi^{(2)}$ structure [10, 12] or to the enhancement of $\chi^{(2)}$ at domain walls as suggested in [18]. However, Čerenkov-type second-harmonic generation can also be observed in an extreme case where a single boundary between two inversely oriented ferroelectric domains is illuminated [19, 20]. In a two-dimensional nonlinear photonic structure (NPS) Čerenkov-type second-harmonic radiation is typically emitted on a cone, which is azimuthally modulated due to the individual form and size of the ferroelectric domains [21, 22] and the polarization properties of the effective nonlinear coefficient [15]. Moreover, additional modulations can also be found on Čerenkov higher-harmonic cones due to the cascaded nature of the generation process [23]. Sum-frequency generation and more complex cascaded nonlinear processes which result in Čerenkov emissions have also been reported [12, 24, 25]. Recent studies have been devoted to enhance the generation process, depending on the combination of the natural Čerenkov and the transverse Raman-Nath condition in one-dimensional periodic nonlinear photonic structures [26]. This enhancement is desirable for potential applications of the Čerenkov emission in analyzing and describing of domain patterns in ferroelectric crystals [20]. In contrast to periodic structures, the process of Čerenkov-type frequency conversion in nonlinear photonic structures with a random distribution of ferroelectric domains is still not fully understood, being attributed either to the broad spectra that verify the longitudinal phase matching, or the enhancement of the $\chi^{(2)}$ nonlinearity at the domain walls [27].

For a better understanding of the nature of this process, and its relation to the domain distribution, we analyze the second-harmonic (SH) intensity of the Čerenkov emission for different angles of incidence of the fundamental wave at different averaged ferroelectric domain sizes in random strontium barium niobate (SBN). Different averaged domain sizes were created by electric poling at room temperature as explained in [9]. Scanning the SH Čerenkov allows for conclusions on the Fourier space representation of the domain spatial distribution. With this technique of **Če**renkov-type **s**econd-harmonic **s**pectroscopy (ČESS), we explain the process of Čerenkov-type second-harmonic generation emission and its relation to the spatial domain distribution in random nonlinear photonic structures.

In this paper, we start by introducing the principle of ČESS in Section 2 and show the experimental setup in Section 3, followed by the results and a comparison with numerical simulations, supported by microscopic domain images in Section 4. We use SBN samples with two different averaged domain sizes. Hereon, the scan experiments are repeated for horizontal and vertical input polarizations addressing specific features of the second-order nonlinear coefficients of SBN. The method of Čerenkov-type SHG spectroscopy is not only a powerful tool to characterize random nonlinear photonic structures but it is also applicable to periodic and quasi-periodic structures as recently published in [26].

2. Principle of Čerenkov-type second-harmonic spectroscopy

In far-field, the second-harmonic intensity is proportional to the square of the Fourier coefficients, which result from the Fourier transform of the spatial distribution of the $\chi^{(2)}$ nonlinearity [26, 28, 29]. For a two-dimensional (2D) $\chi^{(2)}$ structure modulated in the *xy*-plane the SH

#181210 - $15.00 USD Received 5 Dec 2012; revised 15 Feb 2013; accepted 3 Mar 2013; published 28 Mar 2013

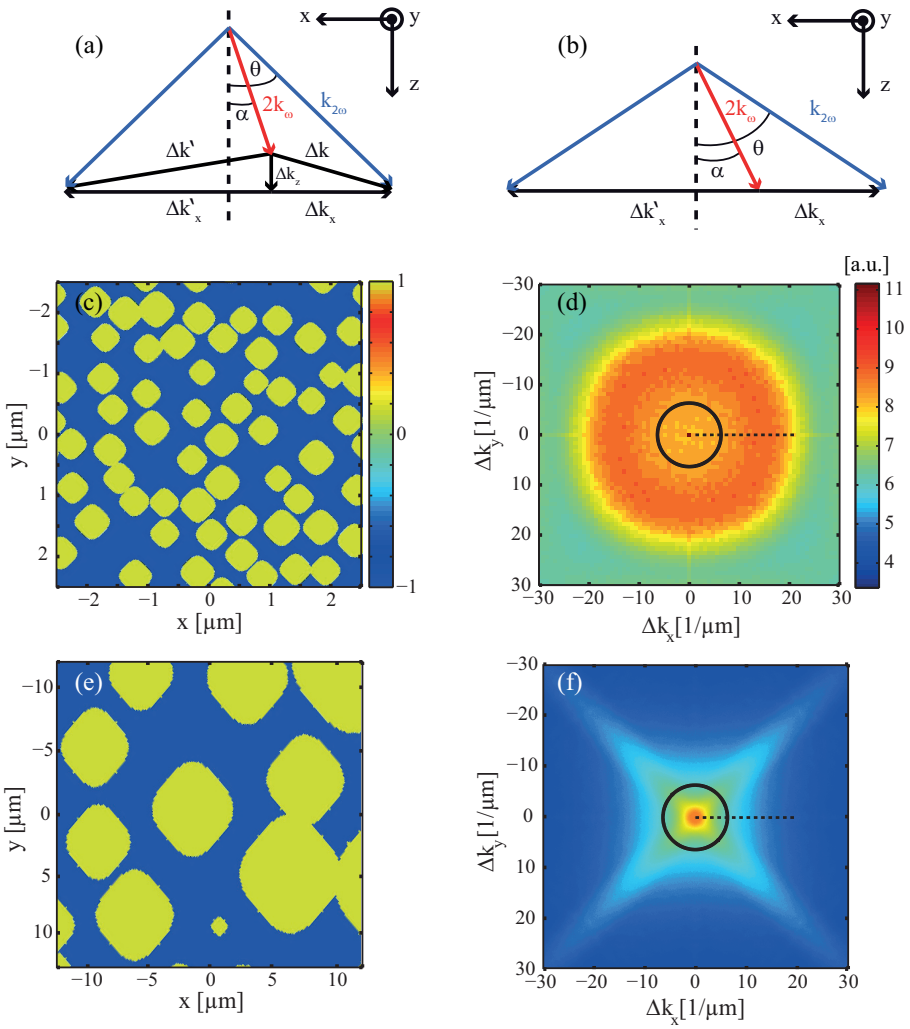

Fig. 1. (a) and (b) Phase matching diagrams for general (left) and Čerenkov-type SH generation, respectively. α is the internal angle of incidence of the fundamental wave and θ the SH internal emission angle. (c) and (e) Modeled real space $s(x,y)$ of random up- and down-domain structure for the two averaged domain sizes of 0.25 μm and 3.5 μm, respectively. (d) and (f) The corresponding spatial Fourier spectrum of the domain patterns $S(\Delta k_x, \Delta k_y)$. The Fourier coefficients involved in Čerenkov SH emission at normal incidence at 600 nm are marked with solid circles. The scan range Δk_x at one side is indicated by dashed lines.

intensity in far-field is

$$I_{\mathrm{SH}} \propto d_{\mathrm{eff}}^2 I_{\mathrm{FW}}^2 L_z^2 |S(\Delta k_x, \Delta k_y)|^2 \mathrm{sinc}^2\left(\frac{\Delta k_z L_z}{2}\right), \tag{1}$$

where I_{FW} is the intensity of the fundamental wave propagating along the z-axis, L_z is the domain length, and $S(\Delta k_x, \Delta k_y)$ is the Fourier spectrum of the domain structure with the transverse phase mismatch vectors $\Delta k_x, \Delta k_y$ in the x- and y-direction [see Figs. 1(a) and 1(b)]. Figure 1(b) shows the corresponding phase-matching diagram of Čerenkov emission in the xz-plane, for

#181210 - $15.00 USD Received 5 Dec 2012; revised 15 Feb 2013; accepted 3 Mar 2013; published 28 Mar 2013

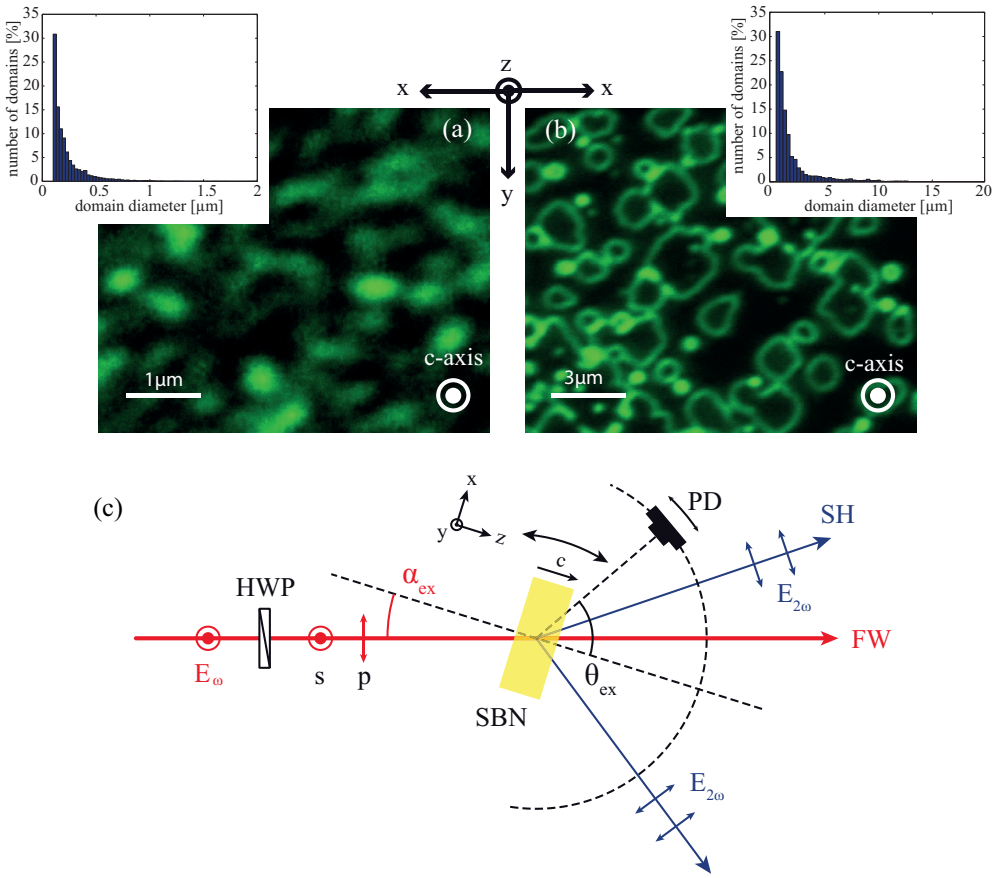

Fig. 2. Disordered ferroelectric domain pattern in as-grown (a) and repoled (b) strontium barium niobate imaged by scanning Čerenkov-type second-harmonic generation microscopy. The green color represent the domain boundaries. The insets depict histograms of the two cases (a) d = 0.36 µm, σ = 0.18 µm, (b) d = 3.01 µm, σ = 2.6 µm. (c) Schematic of the experimental setup. E_ω, $E_{2\omega}$: electric field vectors of the fundamental and second-harmonic waves, HWP: half-wave plate, (s) and (p): vertical and horizontal input polarizations, α_{ex}: external rotation angle, θ_{ex}: external emission angle, PD: photo diode. The second-harmonic signal is measured for each angular position α_{ex} of the sample with the photo diode in the xz-plane.

which $\Delta k_x = k_{2\omega}\sin\theta - 2k_\omega \sin\alpha$, $\Delta k_y = 0$, and $\Delta k_z = 0 = k_{2\omega}\cos\theta - 2k_\omega\cos\alpha$ are the phase mismatch vector components and α is the internal angle of incidence of the fundamental wave and θ the internal second-harmonic emission angle. k_ω, $k_{2\omega}$ denote the wave vectors of the FW and the SH waves. d_{eff} is the effective second-order nonlinear coefficient of the employed configuration. At the Čerenkov angle, $\Delta k_z = 0$ is fulfilled, i.e. the process is phase-matched for the length of a domain. In a homogeneously poled crystal S is nearly zero and Čerenkov light can hardly be measured in contrast to a periodically poled crystal which features a discrete Fourier spectrum [26]. Because the domain pattern is random in our case, the Fourier coefficient $|S(\Delta k_x, \Delta k_y)|$ will be replaced with its average $\langle|S(\Delta k_x, \Delta k_y)|\rangle$, calculated over many domains distributions [30, 31]. Herein, I_{SH} is measured for each angular position α_{ex} of the sample. In this way, $|S(\Delta k_x, \Delta k_y)|$ can be scanned and compared with Fourier spectra numerically calcu-

#181210 - $15.00 USD Received 5 Dec 2012; revised 15 Feb 2013; accepted 3 Mar 2013; published 28 Mar 2013

lated for different domain distributions. In Figs. 1(c) and 1(e), simulated domain structures of a square shape with rounded corners for two different averaged domain sizes are depicted. From the corresponding Fourier spectrum in Figs. 1(d) and 1(f), it is expected that varying the angle of incidence of the fundamental wave leads to a strong angular characteristic asymmetry in the Čerenkov signal intensity in the far-field. Thus, the Čerenkov intensity will increase or decrease continuously, corresponding to the Fourier coefficients considered $|S(\Delta k_x, 0)|$, which are located on the *x*-axis in our treatment here. These are marked with a dashed line [cf. Figs. 1(d) and 1(f)]. We also note that in case of disordered structures for normal incidence of the fundamental wave, the Čerenkov-type second-harmonic generation can be described even by a single-domain model [9, 21]. In this paper, we pursue this idea experimentally by creating different domain size distributions. All results were modeled numerically, including the role of the second-order coefficients for the two characteristic input polarizations, perpendicular (s) and parallel (p) to the plane of incidence. This approach allows fitting the angular intensity in far-field to retrieve the corresponding domain width. This type of Čerenkov spectroscopy provides an unambiguous fingerprint of the domain distribution.

3. Experimental setup and samples with random nonlinear photonic structures

A schematic illustration of the experimental setup for measuring the second-harmonic intensity is depicted in Fig. 2. As a light source, we use ultrashort laser pulses, generated by a laser system consisting of a mode-locked Ti:sapphire oscillator, a regenerative amplifier and an optical parametric amplifier. The repetition rate is 1 kHz, the pulse duration is about $\tau_p = 80$ fs, and the pulse energy amounts to 80 μJ at the wavelength 1200 nm which is used in the experiments. Collimated Gaussian laser pulses with a beam diameter of about 1.5 mm are propagating in the *xz*-plane of the SBN crystal. The light is always linearly polarized, and the polarization orientation of the entering beam is controlled by a proper $\lambda/2$ wave plate for the used wavelength. A $Sr_{0.61}Ba_{0.39}Nb_2O_6$ sample with the dimensions $6.6 \times 6.6 \times 1.6$ mm^3 is employed. The large surfaces perpendicular to the *c*-axis are polished to optical quality. As shown in [9, 32], different domain size distributions can be introduced by applying an electric field along the crystal's polar axis [cf. Figs. 2(a) and 2(b)].

In the experiment, the SBN sample is mounted on a rotation stage which allows us to control the incident angle α_{ex}. The Čerenkov second-harmonic signal is emitted on a cone with the opening angle $\theta_{\text{Ce}}(\lambda, \alpha_{\text{ex}})$. The SH intensity is measured using a silicon photo diode mounted on another rotation stage centered around the crystal in the *xz*-plane [see the insets in Figs. 3(a) and 3(b)]. Both rotation stages have the same rotating axis. In preparation, the crystal was first heated up above the Curie temperature $T_c \approx 70\,^{\circ}$C, and then cooled down without applying an electric field to produce a state similar to an as-grown sample. In order to influence the domain size and form, the sample was subsequently poled and repoled stepwise at room temperature with the same procedure shown in [9, 32]. For this purpose, an electric field was applied along the polar axis by increasing the field in steps of 10 V every 2 s above the coercive field until finally 7.5 kV/cm are reached in one direction to pole the crystal and vice versa to repole it. Figures 2(a) and 2(b) show two experimental images of random domain structures of the SBN sample in two different poling states. The images were obtained by Čerenkov-type second-harmonic generation microscopy on a separate setup described in details elsewhere [20]. Briefly, the output beam of a Ti-Sapphire laser (800 nm, 80 MHz repetition rate, 100 fs pulse duration, 12 nJ pulse energy) is coupled to a commercial laser scanning confocal microscope (LSM 510, Zeiss) and tightly focused by the microscope objective (alpha-Plan-Fluar 100 NA 1.46) to a near diffraction limited spot in the sample. The position of the focus is raster-scanned in the *xy*-plane by a pair of galvanometric mirrors. The intensity of the generated second-harmonic signal is measured by a photomultiplier as a function of the focus

#181210 - $15.00 USD Received 5 Dec 2012; revised 15 Feb 2013; accepted 3 Mar 2013; published 28 Mar 2013

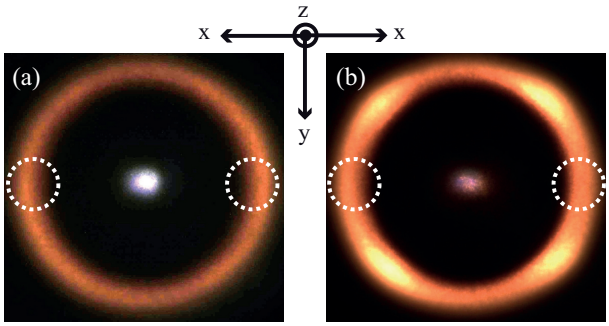

Fig. 3. Experimental photographs of Čerenkov second-harmonic emission for the fundamental wavelength 1200 nm for normal incidence. (a) for unpoled case; (b) for repoled case. The marked positions represent the positions of the measured SH intensities.

position, using the standard transmission mode of the microscope. As shown in [20], a strong Čerenkov-type second-harmonic generation is obtained only when the focal spot is crossing a domain wall, which allows precise domain visualization. For a quantitative evaluation, the insets in Figs. 2(a) and 2(b) depict histograms of normalized number of domains versus domain size for the unpoled and repoled cases, respectively. Those histograms have been obtained by analyzing several microscopic images taken with the same method for each case and provide information about the actual domain size distribution. For the unpoled case, the corresponding distribution is of the mean value $d = 0.36$ μm and standard deviation $\sigma = 0.18$ μm. The repoled case obviously shows larger domains of a mean value 3.01 μm and standard deviation 2.6 μm. These two size scales of the ferroelectric domains lead to different Čerenkov SH emissions in the far-field. Figures 3(a) and 3(b) show the typical Čerenkov SH emissions at normal incidence of the fundamental wavelength 1200 nm. Clearly, no modulation is observed on the Čerenkov ring for the unpoled case [cf. Fig. 3(a)] [22]. This can be expected from the corresponding Fourier coefficients, which verify the Čerenkov phase-matching condition and are marked with a solid circle in Fig. 1(d). After two poling cycles, larger and more clearly defined domains are formed in the SBN crystal as shown in Fig. 2(b). Again, the corresponding SH emission pattern at the fundamental wavelength 1200 nm is shown in Fig. 3(b). The modulation on the SH ring in this case is attributed to the individual domain shape [22] and can also be seen in Fig. 1(f). In the experiment, the SH intensity is measured within the *xz*-plane for each angular position α_{ex} of the sample. The sample is rotated in an angular range of $-60^\circ \leq \alpha_{ex} \leq 60^\circ$, corresponding to transverse phase mismatches of $|\Delta k_x| = 1.9 - 21\ \mu\text{m}^{-1}$ and $\Delta k_y = 0$. Since the domain shape is symmetric, no significant changes are expected when rotating the sample 90° around the *z*-axis. Measuring the SH intensity in the *xz*-plane is almost equivalent to the one-dimensional case, represented in [26]. However, the presented method can also be used to analyze nonlinear photonic structures with asymmetric domains like one dimensional periodically poled crystals by scanning the SH signal in different planes. We distinguish between two characteristic input polarizations, horizontal and vertical, because the effective second-harmonic nonlinear coefficients take different forms in each case. The experiments are performed with an unpoled and repoled sample, respectively, exhibiting the average domain size indicated in Fig. 2.

4. Retrieving the averaged domain sizes by ČESS

A scan experiment for an unpoled SBN sample, corresponding to the domain image shown in Fig. 2(a), is depicted in Fig. 4(a). As shown, at normal incidence the external Čerenkov angle is about 37° with respect to the *c*-axis and this angle increases while rotating the crystal.

#181210 - $15.00 USD Received 5 Dec 2012; revised 15 Feb 2013; accepted 3 Mar 2013; published 28 Mar 2013

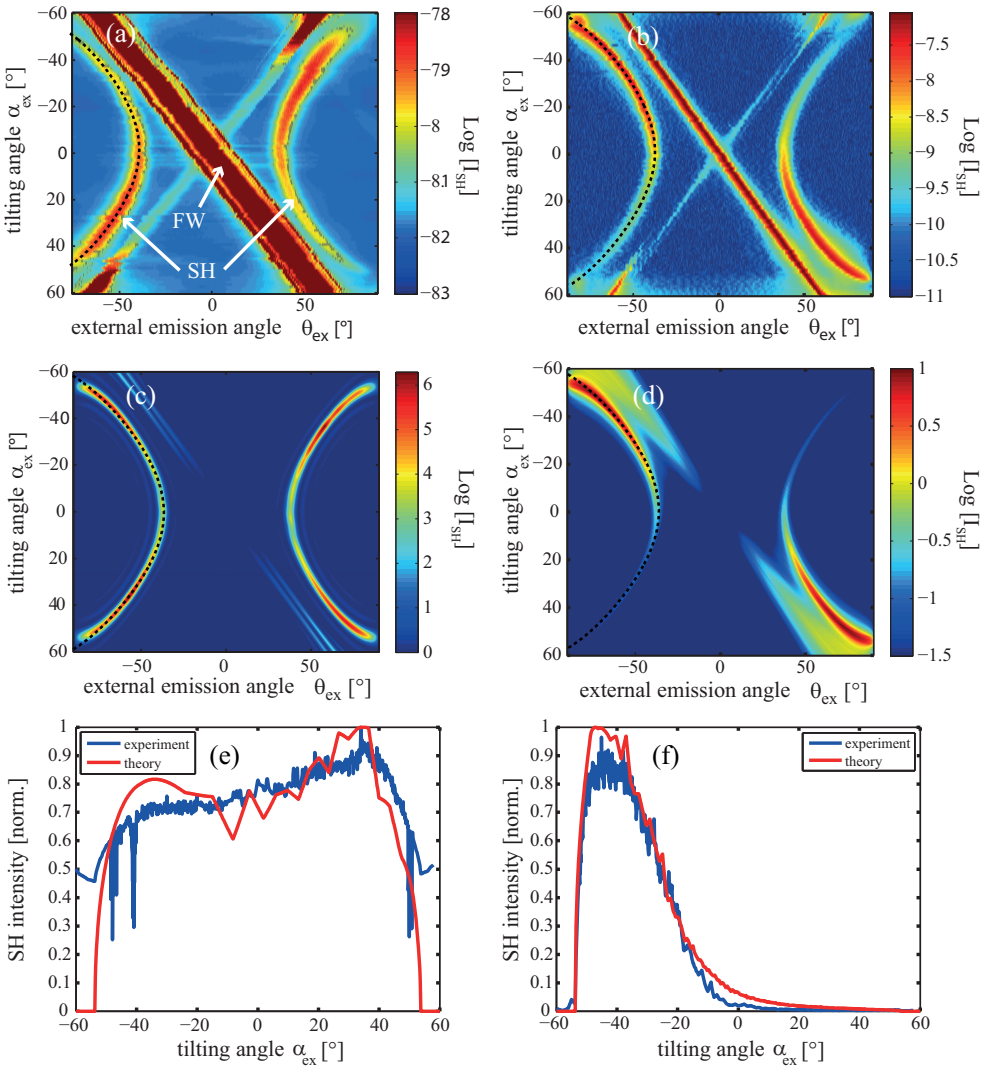

Fig. 4. (a) and (b) Experimentally measured Čerenkov second-harmonic signal at 600 nm while rotating the unpoled (a) and repoled (b) SBN sample, respectively for an s-polarized fundamental wave. (c) and (d) Numerically simulated far-field intensity of the second-harmonic signal as a function of the incidence angle α_{ex} for an average domain width of 0.25 μm (c) and 3.5 μm (d). (e) and (f) Second-harmonic intensities emitted at the Čerenkov angle on one side of the crystal marked with dashed arcs in (c) and (d) as a function of the tilting angle.

#181210 - $15.00 USD Received 5 Dec 2012; revised 15 Feb 2013; accepted 3 Mar 2013; published 28 Mar 2013

At the same time, the SH Čerenkov intensity becomes asymmetric and increases with increasing transverse phase mismatch Δk_x or equivalently with increasing negative tilting angle. This means that the largest Fourier coefficients are on a ring in the Fourier space with a radius larger than the one for normal incidence as clearly shown in Fig. 1(d). The experiment has been repeated for a repoled sample, prepared in the same manner as explained above, corresponding to the domain image depicted in Fig. 2(b). The result is shown in Fig. 4(b). In this case, in contrast to an unpoled SBN crystal, the Čerenkov intensity increases with decreasing transverse phase mismatch, i.e. increasing positive tilting angle. This indicates large Fourier coefficients close to the origin of the Fourier space [see Figs. 1(e) and 1(f)], what in turn means large domains as shown in the domain image in Fig. 2(b). The line perpendicular to the fundamental wave is due to the reflection at the sample's edges.

In order to analyze the intensity behavior for each case, the SH Čerenkov intensity distribution inside the sample can be obtained by Eq. (1) with the corresponding effective nonlinear coefficient. For that, we assumed a 2D random domain structure in the *xy*-plane with a domain width described by Gaussian distribution [12, 31] of an average domain width d and standard deviation σ and a square domain shape [22, 33]. No modulation in the *z*-direction is supposed at this point. Moreover, the Frensel losses have also been taken into account for each polarization case. For a vertical polarization of E_ω, the effective nonlinear coefficient is given by $d_{\text{eff}} = d_{31}\sin\theta$. The calculated Čerenkov intensity as a function of the tilting and emission angles is depicted in Figs. 4(c) and 4(d) for the unpoled (small domains) and repoled (large domains) sample, respectively. For the unpoled case [Figs. 4(a) and 4(c)], the best agreement with the measured intensity and the microscopic domain image [cf. Fig. 2(a)] is with the chosen parameters for the averaged domain $d = 0.25$ μm with a standard deviation of $\sigma = 0.07$ μm, averaged over possible 200 realizations of domain structure. For the repoled case [Figs. 4(b) and 4(d)], the averaged domain width is larger and $d = 3.5$ μm with $\sigma = 0.7$ μm, which fits well to Fig.2(b) and previous experimental results [9]. This can be seen more clearly when plotting the SH intensity at the Čerenkov angle for each case as a function of the tilting angle only [see Figs. 4(e) and 4(f)]. In Figs. 4(e) and 4(f), only one side is plotted exemplary. The resulted distribution by the numerical simulation differs slightly from those of the histograms. This can be attributed to the fact, that our simulation did not consider the agglomeration, which can be seen in the domain structures. Furthermore, the microscopic Čerenkov-type SH images represent a small area and a thin slice of the whole sample. In spite of that, the numerical simulation fits very well the measured SH intensity. Now, for p-polarization, the Čerenkov intensity behavior seems to be the same for unpoled and repoled cases. In both cases, the SH intensity increases with decreasing the transverse phase mismatch. The measured intensity is depicted in Fig. 5 for the unpoled state. The results exhibit a minimum in the Čerenkov second-harmonic intensity at the tilting angle of about $\mp 14^\circ$, which can be attributed to the effective nonlinear coefficient d_{eff} for p-polarized light. In the case of normal incidence, d_{eff} in the *xz*-plane is described only by $d^z_{\text{eff}} = d_{31}$. When rotating the sample around the *y*-axis, d_{eff} takes the form $(d_{31}\cos^2\alpha + d_{33}\sin^2\alpha)\sin\theta + 2d_{15}\cos\alpha\sin\alpha\cos\theta$. The total SH signal consists of these three contributions and depends on whether contributions from both of these processes add coherently or not. The SH intensity behavior for a p-polarized fundamental wave indicates coherent superposition of these three SH contributions in this configuration, where the longitudinal phase-mismatch is zero and the phase velocities are matched over the whole domain length. This characteristic trend of the SH Čerenkov intensity for this polarization is calculated with the corresponding effective nonlinear coefficient. It is worth to mention here that the position of the intensity minimum depends on the ratios of the involved nonlinear tensor elements d_{33}/d_{15}, d_{33}/d_{31} which are chosen to be about 2 [34]. However, the scan experiments for p-polarized fundamental light show a broad intensity minimum. For this case, the same param-

#181210 - $15.00 USD Received 5 Dec 2012; revised 15 Feb 2013; accepted 3 Mar 2013; published 28 Mar 2013

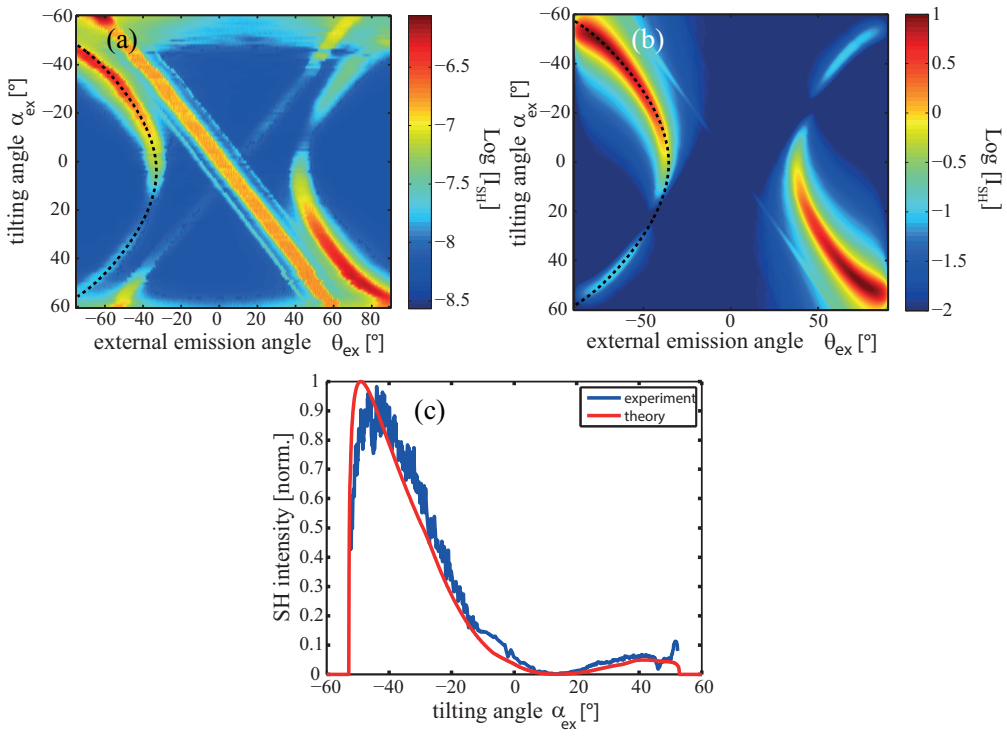

Fig. 5. (a) Experimentally measured Čerenkov second-harmonic signal at 600 nm while rotating the unpoled SBN sample for p-polarized fundamental light. (b) Numerically simulated far-field intensity of the second-harmonic signal as a function of the tilting angle α_{ex} for an average domain width of 0.25 μm. (c) Second-harmonic intensity emitted at the Čerenkov angle on one side of the crystal, marked with dashed arcs in (a) and (b). as a function of the tilting angle α_{ex}.

eters as for the s-polarization and the unpoled case are taken to describe the SH intensity traces for p-polarization. Figures 5(b) and 5(c) show a very good correspondence with the measured data. The experiment shows no significant influence of the Fourier coefficient *S* on the intensity traces because of the dominant effect of the effective nonlinear coefficient. This can be explained by the extraordinary polarization component in the effective nonlinear coefficient for p-polarization, which is naturally larger than the ordinary one in the case of s-polarization.

5. Conclusion

In conclusion, we have demonstrated significant features of Čerenkov second-harmonic emission in two-dimensional random nonlinear photonic structures. These features allow determining the mean width of the ferroelectric domains by measuring the second-harmonic intensity at the Čerenkov angle for different incidence angles, i.e. mapping the spatial Fourier spectrum of the domain patterns. This method was applied for two different domain distributions and two characteristic polarizations of the fundamental light, proving its versatility. For s-polarized light, two different SH intensity traces were measured, numerically analyzed, and compared with microscopic images. For p-polarized light, no significant changes in the SH intensity distribution was measured when changing the domain size due to the dominant effect of the effective nonlinear coefficient in this case. All experimental results are in excellent agreement with

#181210 - $15.00 USD Received 5 Dec 2012; revised 15 Feb 2013; accepted 3 Mar 2013; published 28 Mar 2013

the applied model.

Acknowledgment

Financial support of Deutsche Forschungsgemeinschaft and Open Access Publication Fund of University of Münster is gratefully acknowledged.

#181210 - $15.00 USD Received 5 Dec 2012; revised 15 Feb 2013; accepted 3 Mar 2013; published 28 Mar 2013